Kinesin Kip2 enhances microtubule growth *in vitro* through length-dependent feedback on polymerization and catastrophe

Anneke Hibbel, Aliona Bogdanova, Mohammed Mahamdeh, Anita Jannasch, Marko Storch, Erik Schäffer, Dimitris Liakopoulos, Jonathon Howard

DOI: http://dx.doi.org/10.7554/eLife.10542

Cite as: eLife 2015;10.7554/eLife.10542

Received: 3 August 2015
Accepted: 17 November 2015
Published: 18 November 2015

Title:

Kinesin Kip2 enhances microtubule growth *in vitro* through length-dependent feedback on polymerization and catastrophe

Authors:

Anneke Hibbel[1], Aliona Bogdanova[1], Mohammed Mahamdeh[2], Anita Jannasch[1,4], Marko Storch[3], Erik Schäffer[4], Dimitris Liakopoulos[5] & Jonathon Howard[2]

Affiliations:

[1]Max Planck Institute of Molecular Cell Biology and Genetics, Dresden, Germany

[2]Department of Molecular Biophysics & Biochemistry, Yale University, New Haven, CT, USA

[3]Department of Life Sciences, Imperial College London, UK

[4]ZMBP, Eberhard-Karls-Universität Tübingen, Germany

[5]CRBM-CRNS, Montpellier, France

Competing interests:

The authors declare that no competing interests exist.

To whom correspondence should be addressed: Jonathon Howard, Department of Molecular Biophysics & Biochemistry, Yale University, 266 Whitney Avenue, New Haven, CT 06511. Tel: (203) 432-7245. Fax (203) 432-8492. Email: jonathon.howard@yale.edu

Running title: **Budding yeast kinesin Kip2 paves its own way on microtubules**

Abstract

The size and position of mitotic spindles is determined by the lengths of their constituent microtubules. Regulation of microtubule length requires feedback to set the balance between growth and shrinkage. Whereas negative feedback mechanisms for microtubule length control, based on depolymerizing kinesins and severing proteins, have been studied extensively, positive feedback mechanisms are not known. Here we report that the budding yeast kinesin Kip2 is a microtubule polymerase and catastrophe inhibitor *in vitro* that uses its processive motor activity as part of a feedback loop to further promote microtubule growth. Positive feedback arises because longer microtubules bind more motors, which walk to the ends where they further reinforce growth and inhibit catastrophe. We propose that positive feedback, common in biochemical pathways to switch between signaling states, can also be used in a mechanical signaling pathway to switch between structural states, in this case between short and long polymers.

Results and Discussion

The budding yeast kinesin Kip2 promotes microtubule growth *in vivo*. Deletion of this kinesin results in nuclear migration defects, and the phenotype is associated with shorter, less abundant cytoplasmic microtubules (Cottingham and Hoyt, 1997; Huyett et al., 1998; Miller et al., 1998; Caudron et al., 2008). Conversely, Kip2 over-expression results in hyper-elongated cytoplasmic microtubules (Carvalho et al., 2004). The stabilization of microtubules by Kip2 is thought to be indirect and a consequence of Kip2 transporting the growth regulator Bik1 (Clip170) to microtubule plus ends (Carvalho et al., 2004; Caudron et al., 2008).

To test whether Kip2 alone can promote microtubule growth, the activity of full-length, purified Kip2 was measured in dynamic microtubule assays using porcine tubulin in the presence of ATP (Gell et al., 2010; 2011) (Figure 1A). Within 10 minutes, Kip2 (Figure 1B,C), as

well as Kip2-eGFP (Figure1-figure supplement 1A), strongly increased the length of freshly polymerized microtubules (p < 0.0001, Welch's unpaired t-test, please refer to Table 1 for porcine microtubule parameter values). The effect of Kip2 on microtubule length was almost completely inhibited when ATP was replaced by the non-hydrolyzable ATP analog AMP-PNP (Figure 1C, blue markers, p < 0.0001), showing that growth promotion requires ATP hydrolysis. To quantify how Kip2 influences microtubule dynamics, we drew kymographs from the time-lapse images of the dynamic microtubule assay (Figure 1D). Kip2 increased the growth rate of microtubules (the slope of the growing microtubule in the kymograph) 2.9-fold (Figure 1E). In addition, Kip2 reduced the frequency of catastrophe (the transition between growth and shrinkage phases) approximately 10-fold (Figure 1F). Kip2 did not affect the shrinkage rate (Figure1-figure supplement 1B), but increased the frequency of rescue (the transition between shrinkage and growth phases, Figure1-figure supplement 1C, p < 0.005). All dynamic data on porcine tubulin are contained in Table 1. Rescue is not expected to have a large effect on microtubule length in our assays. This is because at lower Kip2 concentrations (< 10 nM), the average distance shortened following catastrophe (the shrinkage rate divided by the rescue frequency) is greater than the average distance grown before catastrophe (the growth rate divided by the catastrophe frequency) so microtubules usually shrink all the way back to the seed (as expected by theory, Verde et al. 1992). On the other hand, at higher Kip2 concentrations, catastrophes are so rare that microtubules are expected to be very long before they catastrophe (>18 μm for [Kip2] ≥ 10 nM). Consistent with these arguments, the measured increase in microtubule length accorded with the effects of Kip2 on the growth rate and the catastrophe frequency alone (Figure 1 C, red line). The half-maximal stimulation of polymerization and inhibition of catastrophe occurred at ≈7 nM Kip2. Given that the cellular concentration of Kip2 is ≈25 nM (Ghaemmaghami et al., 2003), these results show that Kip2 affects microtubule dynamics *in vitro* at physiologically relevant concentrations.

To exclude potentially confounding effects introduced by using fluorescently labeled porcine brain tubulin, as well as to confirm that Kip2, which is a yeast protein, has the same activity on its conspecific protein, we repeated the dynamic microtubule assays with unlabeled yeast tubulin (Widlund et al., 2012) and DIC microscopy (Figure1-figure supplement 2A, please refer to Table 2 for yeast microtubule parameter values). Consistent with our porcine tubulin results, Kip2 increased the yeast microtubule growth rate by 2.3-fold and inhibited catastrophe 20-fold (Figure1-figure supplement 2B,C). The half-maximal stimulation of polymerization and inhibition of catastrophe for yeast tubulin occurred at ≈12 nM Kip2, similar to the concentration at which Kip2 regulates porcine brain microtubules. In summary, Kip2 is a microtubule polymerase and anti-catastrophe factor *in vitro*, and does not require additional proteins such as Bik1 for these activities. We defer discussion of a potential role for Bik1 until the end of the manuscript.

To gain insight into the mechanism of Kip2's polymerase and anti-catastrophe activities we determined how Kip2 affects microtubule assembly and disassembly kinetics. By measuring the rate of growth of porcine microtubules from GMPCPP seeds over a range of tubulin concentrations (Figure1-figure supplement 3A), we found that Kip2 doubled the effective tubulin association rate constant (k_{on}, the rate that tubulin is stably incorporated into the microtubule lattice) to 1.5 $\mu M^{-1} \cdot s^{-1}$ (at the plus end) from 0.7 $\mu M^{-1} \cdot s^{-1}$ in the absence of Kip2. In addition to accelerating the net addition of subunits, Kip2 also facilitated microtubule nucleation off the seeds, with robust growth observed at tubulin concentrations as low as 4 μM, compared to 10 μM in the absence of Kip2 (Figure1-figure supplement 3A). Thus, Kip2 acted like a nucleation factor in analogy to XMAP215 (Wieczorek et al., 2015). The increased growth rate in the presence of Kip2 is expected to have only a modest effect on catastrophe because doubling the rate of microtubule growth by doubling the tubulin concentration only decreased the catastrophe frequency about 2-fold (Gardner et al. 2011; Walker et al. 1988). Our observation that the

99 catastrophe frequency decreased ten-fold might be explained by our finding that 40 nM Kip2
100 decreased the rate of dissociation of GMPCPP-tubulin subunits from GMPCPP microtubules
101 (k_{off}) approximately 3-fold (Figure1-figure supplement 3B). If GMPCPP-tubulin acts as an analog
102 for GTP-tubulin (Hyman et al. 1992), then a decrease in k_{off} is expected to stabilize the GTP cap
103 and therefore inhibit catastrophe (Bowne-Anderson et al. 2013; Coombes et al. 2103; Margolin
104 et al. 2011). Thus, the increase in k_{on} and the decrease k_{off} likely account for most of the
105 decrease in the catastrophe frequency.

106 To determine how Kip2 targets the plus ends of microtubules, we characterized its
107 biophysical properties in single-molecule motility assays (Figure 2A). Kymographs revealed that
108 in 1 mM ATP, single Kip2-eGFP molecules associated with GMPCPP-stabilized porcine
109 microtubules along the lattice and walked processively towards the plus end of the microtubule
110 (Figure 2B, Figure2-figure supplement 1A). The velocity was 5.0 ± 0.9 μm/min at 28°C (mean ±
111 SD, *n* = 674 traces). The average run distance before dissociating was 4.1 ± 0.3 μm (mean ±
112 SE, *n* = 217, Figure2-figure supplement 1B). A similar velocity was observed by Roberts et al.
113 (2014), though the run distance was shorter (1.2 μm). At the plus end, Kip2-GFP resided for 30
114 ± 26 s before dissociating (mean ± SD, *n* = 40, Figure 2D, Figure2-figure supplement 1C),
115 leading to an accumulation of up to 12 Kip2-eGFP molecules at the plus-end, based on the
116 fluorescence intensity (Figure 2B). When the ATP was replaced by the non-hydrolyzable analog
117 AMP-PNP, Kip2-eGFP tightly bound to the lattice and did not translocate (Figure 2C). Kip2-
118 eGFP moved slower on dynamic microtubules (2.1 ± 0.89 μm/min), but this velocity is still
119 greater than the microtubule's growth speed, so Kip2-eGFP was able to catch up to the growing
120 ends of dynamic microtubules, and track them (Figure 2E). Based on these properties, we
121 conclude that Kip2's mechanism differs from that of the well-studied microtubule polymerase
122 XMAP215. XMAP215 targets ends by diffusion and capture (Brouhard et al. 2008, Widlund et al.
123 2011), increases both k_{on} and k_{off} (Brouhard et al. 2008) and has little effect on catastrophe

(Zanic et al. 2013). Furthermore, Kip2's ATPase activity is necessary for its activity, while XMAP215 is not an ATPase. Thus, Kip2 is a unique regulator of microtubule dynamics. Two models for growth promotion can be envisaged. Kip2 may increase growth rates by shuttling tubulin to the microtubule plus-end, locally increasing the tubulin concentration. Alternatively, it could promote microtubule growth by acting as a processive polymerase while at the plus-end, like XMAP215 (Brouhard et al. 2008). More work will be required to distinguish between these and other mechanisms.

To probe the mechanical properties of Kip2, we measured the stall force of single-molecules using optical tweezers (Jannasch et al., 2013). Positional tracking of single-Kip2-powered microspheres moving along GMPCPP-stabilized porcine microtubules as a function of time under constant load revealed a zero-force speed of 4.0 ± 0.5 μm/min at 24.5°C, similar to that measured in the TIRF assays. Kip2 stalled at a force of 0.81 ± 0.04 pN (Figure 3A) and showed a nearly linear force-velocity relation with increased velocity as the assisting force was increased (Figure 3C). At high forces, the motor often slipped along the microtubule in the direction of the applied force without detaching (Figure 3B). The ability to switch from the slip state to the normal translocation mode is thought to increase processivity by linking together several shorter run lengths (Jannasch et al., 2013). Thus, Kip2 is a processive, low-force motor with long run-lengths and end-residence times. The low force supports the idea that individual Kip2 motors transport small cargos such as dynein, Bik1 and other molecules (Roberts et al., 2014) rather than organelles, though it is possible that multiple Kip2s could cooperate to move larger cargos. The strong localization to the microtubule plus end accords with Kip2 being a regulator of microtubule dynamics.

The low force and high processivity of Kip2 are reminiscent of the microtubule depolymerase Kip3, in the kinesin-8 family (Jannasch et al., 2013; Varga et al., 2006). Kip3 is a length-dependent depolymerase that uses an antenna mechanism to preferentially localize to

149 the plus ends of longer microtubules (Varga et al., 2009). We therefore tested whether the
150 promotion of microtubule growth by Kip2 is length-dependent (Figure 4A,B). Without Kip2,
151 microtubules grew at a length-independent, constant rate (black circles, p = 0.06, Student's t-
152 test on a linear fit to the raw data). By contrast, at low (1-2 nM) and intermediate (5-10 nM) Kip2
153 concentrations, long microtubules grew faster than short microtubules ($p < 0.0001$). At high Kip2
154 concentrations (20-40 nM), microtubules again grew at a constant, length-independent rate
155 (green circles, p = 0.36); however, at these high Kip2 concentrations we expect all the length
156 dependence to be in the first few microns, which is not well resolved in these experiments (see
157 green fitted line). Analysis of yeast microtubule growth rates as a function of microtubule length
158 yielded similar results (Figure4-figure supplement 1A). Thus, Kip2 is a length-dependent
159 microtubule polymerase.

160 To test whether Kip2 also prevents catastrophe in a length-dependent manner, we
161 measured porcine microtubule lengths at the moment of catastrophe. To compare the
162 catastrophe frequency at short versus long microtubule lengths, we set a cut-off length at 4 μm,
163 which equals the run-length of Kip2. Using data from the dynamic microtubule assays (Figure
164 1), we measured the catastrophe length for short microtubules as the total distance that
165 microtubules grew while their length (including seed) was shorter than 4 μm divided by the
166 number of catastrophes that occurred at lengths < 4 μm. For long microtubules, we summed the
167 distance that microtubules grew while longer 4 μm (final length minus 4 μm) and divided by the
168 number of catastrophes that occurred at lengths > 4 μm (Figure 4C, inset). In the absence of
169 Kip2, the catastrophe length of shorter microtubules was less than that of longer microtubules
170 (Figure 4C, 0 nM Kip2, $p < 0.05$, Welch's unpaired t-test). This reflects an increase in
171 catastrophe frequency with length, as expected due to microtubule aging (Gardner et al., 2011).
172 By contrast, at 5 nM Kip2, the catastrophe length of longer microtubules was greater than that of
173 shorter microtubules (Figure 4C, $p < 0.0001$). This indicates that the inhibition of catastrophe is

a length-dependent. Similar results were obtained for yeast microtubules at 10 nM Kip2 (Figure4-figure supplement 1B, $p < 0.0001$). Thus, in the absence of Kip2, catastrophe frequency increased with increasing microtubule length, whereas in the presence of Kip2 catastrophe frequency decreased with increasing microtubule length. Thus, both the increase in microtubule growth rate and the prevention of catastrophe by Kip2 increase with increasing microtubule length.

Summarizing our results, we have found that budding yeast kinesin Kip2 promotes microtubule growth *in vitro* in a length-dependent manner. Because the rate at which Kip2 translocates exceeds the speed of microtubule growth, Kip2 catches up with the growing end of the microtubule (Figure 2E) where it promotes growth and inhibits catastrophe. As a consequence, this length dependence leads to positive feedback: the longer the microtubule, the greater the number of motors that land on it (the microtubule acts as an antenna), the more motors reach the plus end, and the higher the growth rate and lower the catastrophe frequency. This in turn will lead to longer microtubules, which attract more Kip2 etc. Thus, we expect that once a microtubule is long enough, it will effectively “escape” catastrophe and keep growing almost indefinitely, switching from a catastrophe length of only a few microns in the absence of Kip2 to a length ≥ 40 μm at high Kip2 concentrations (Figure 4C, Table 1). In this sense, Kip2 “paves its own way”. Thus, by combining processivity with polymerase activity, Kip2 can perform an elementary “computation”, which switches short microtubules to long ones. This computation differs from that performed by kinesin-8, a length-dependent depolymerase, which stabilizes microtubule length through negative feedback (Gupta et al., 2006; Mayr et al., 2007; Stumpff et al., 2008; Su et al., 2013; Varga et al., 2006; 2009).

We propose that this positive feedback mechanism may operate *in vivo* and account for the phenotype of Kip2 deletion, which is a reduction in length and number of cytoplasmic microtubules. First, *in vivo* the rate at which Kip2 translocates exceeds the rate of microtubule growth; the respective rates are 6.6 μm/min (Carvalho et al., 2004) and 2.3 μm/min (Caudron et

al., 2008). Second, the run-length of Kip2 (≈4 μm) exceeds the length of cytoplasmic microtubules (≈2 μm (Caudron et al., 2008)). Taken together, these two observations imply that almost every Kip2 that lands on a microtubule will reach the growing plus-end. By promoting growth and inhibiting catastrophe, Kip2 can deliver cytoplasmic dynein (Roberts et al. 2014) to the distal cortex of the growing daughter bud before the microtubules catastrophe.

While the polymerase and anti-catastrophe activities can account for the deletion phenotype of Kip2, it is not obvious why microtubule hyper-elongation when Kip2 is overexpressed should require Bik1 (Carvalho et al., 2004). We propose that Bik1 may be required to increase Kip2's processivity *in vivo*. Feedback can only operate if the run length exceeds the microtubule length. In our *in vitro* assays, the Kip2 run length was ≈4 μm, whereas that measured by Roberts et al. (2014) was only ≈1 μm. We do not know why there is a difference as the assay buffers are similar. Importantly, though, Roberts et al. (2014) found that Bik1 could increase Kip2's run length 3-4 fold (in the presence of Bim1). Therefore, if the run length of Kip2 *in vivo* is short, then the requirement for Bik1 in the over-expression assays may be due to Bik1 acting as a processivity factor that increases the run length, thereby allowing more Kip2 to reach the end where it enhances microtubule growth.

Methods

Protein purification and preparation

Porcine brain tubulin was purified and labeled with tetramethylrhodamine or Alexa Fluor 488 (Invitrogen) according to the standard protocols, as previously described (Gell et al., 2011). Preparation of GMPCPP-stabilized microtubule seeds was performed as previously described (Gell et al., 2010). Full-length 6xHis-Kip2 and 6xHis-Kip2-eGFP were expressed in SF+ cells using baculovirus expression and purified using affinity chromatography over 1 ml His-affinity columns (GE Healthcare). Cells were lysed in 50 mM NaH_2PO_4, 300 mM NaCl, 0.1% Tween-20, 10 mM imidazole, protease inhibitors, 2 mM Mg-ATP, at pH = 8.0. The wash buffer consisted of 50 mM NaH_2PO_4, 300 mM NaCl, 100 mM imidazole, 2 mM Mg-ATP, at pH = 8.0. The elution buffer consisted of 50 mM NaH_2PO_4, 300 mM NaCl, 300 mM imidazole, 2 mM Mg-ATP, at pH = 8.0. Affinity column purification success was checked by SDS-PAGE and Western blot using anti-6xHis antibody (Genscript). Next, the 6xHis-tags were cleaved from the protein using PreScission protease (GE Healthcare). The protease was added to the 300 mM imidazole elution fraction in a 1:50 dilution and incubated overnight on a rotary wheel at 4℃. Protein stability was confirmed by SDS-PAGE and enzymatic cleavage of the 6xHis-tag from the protein of interest by Western blot using anti-6xHis-antibody. Finally, Kip2 and Kip2-eGFP were purified to homogeneity by gel filtration over a Sephadex 200 column which was pre-washed with protein storage buffer: 1x BRB80 (80 mM PIPES, 1 mM $MgCl_2$, 1 mM EGTA, pH 6.8) supplemented with 10% glycerol, 1 mM Mg-ATP, 1 mM dithiothreitol (Figure1-figure supplement 4). Final protein purity was checked by mass spectroscopy at the MPI-CBG in house mass spectroscopy facility. Protein concentration was determined by Bradford assay and purified proteins were snap-frozen using liquid nitrogen and stored at -80℃.

Microscopy assays and imaging conditions.

The dynamic microtubule assay for dynamic growth of Alexa Fluor 488-labeled tubulin from

241 tetramethylrhodamine-labeled GMPCPP-stabilized porcine tubulin seeds were imaged by TIRF
242 microscopy as described previously (Gell et al., 2010). The imaging buffer contained 1x BRB20
243 (20 mM PIPES, 1 mM $MgCl_2$, 1 mM EGTA, pH 6.8) supplemented with 100 mM KCl, 20 mM
244 glucose, 20 µg/ml glucose oxidase, 8 µg/ml catalase, 0.1 mg/ml casein, 1 mM dithiothreitol,
245 0.001% tween-20, 1 mM GTP and 1 mM Mg-ATP or AMP-PNP. The single-molecule motility
246 assay on tetramethylrhodamine-labeled GMPCPP-stabilized tubulin seeds imaged by TIRF
247 microscopy was described previously (Gell et al., 2010). For all experiments, the imaging buffer
248 contained no added GTP. Imaging was performed with an Andor iXon camera on a Zeiss
249 Axiovert 200M microscope with a Zeiss ×100/1.46 plan apochromat oil objective and standard
250 filter sets. An objective heater (Zeiss) was used to warm the sample to 28 °C.
251 The rate of photobleaching in our TIRF assays was low. In the AMP-PNP experiments
252 (e.g. Figure 2C), the mean time to bleaching of Kip2-eGFP was 249 ± 68 s (mean ± SD, n = 10).
253 Given that the average run length of 4.1 µm corresponds to a run time of 82 s (at 50 nm/s), we
254 expect bleaching to have only a small effect on the measured run times. Similarly, bleaching will
255 have little effect on the end residence times. The low rate of photobleaching accords with our
256 earlier quantification of photobleaching (Varga et al. 2009).
257 Differential interference contrast microscopy was described previously (Bormuth et al.,
258 2007). All experiments were performed at least three times on three different days. Image
259 analysis was performed by creating kymographs of microtubule growth events in ImageJ. For
260 growth and shrinkage rates, typically > 20 microtubules were measured, and the mean and
261 standard error of the mean (SE) are reported in the text and Figures. For the catastrophe
262 frequency, we divided the total number of events by the total observation time. For the rescue
263 distance, we divided the total observed distance that microtubules shrank by the total number of
264 rescue events. The relative error (SE) was estimated as the inverse of the square root of the
265 number of events. This assumes that the catastrophe and rescue events are single-step

(Poisson) processes. However, if the events are multistep (e.g. from a gamma distribution), as is known to be the case for catastrophe (Gardner et al., 2011), then the actual SE is smaller than the calculated one.

Optical tweezers assay preparation

Flow-cell construction and immobilization of GMPCPP-stabilized porcine microtubules were performed as previously described (Jannasch et al., 2013). The imaging buffer for optical tweezer experiments contained 1xBRB20 supplemented with 100 mM KCl, 20 mM glucose, 20 µg/ml glucose oxidase, 8 µg/ml catalase, 0.1 mg/ml casein, 0.5% b-mercaptoethanol, 1 mM Mg-ATP. The channels were rinsed with 20 µl imaging buffer with Kip2-functionalized microspheres. For the Kip2-functionalized microspheres, carboxylated polystyrene microspheres (mean diameter 0.59 µm, Bangs Lab.) were bound covalently to anti-GFP antibody via a 3 kDa polyethylene glycol (PEG) linker, which, in turn, bound to the C-terminal eGFP of Kip2-eGFP-6xHis, as previously described (Jannasch et al., 2013). The measurements were performed at 24.5 °C and under single-molecule concentrations where only 1 out of 4 microspheres showed motility.

Optical tweezers trapping experiments

Measurements were performed in a single beam optical tweezers setup as previously described (Schäffer et al., 2007; Bormuth et al., 2009; Jannasch et al., 2013). All measurements were done with a trap stiffness of 0.03 pN/nm. The optical trap is calibrated by analysis of the height-dependent power spectrum density as described previously (Tolić-Nørrelykke et al., 2006). The force-velocity curve was measured using the constant-force mode. In this mode, the trapping laser was moved with a piezo-mirror relative to the sample with an update rate of 200 Hz. Overall, we measured and analyzed the motion of 11 different single Kip2-eGFP-6xHis molecules. Data analysis was previously described (Jannasch et al., 2013).

List of figures and tables

Figure 1

292 Figure1-figure supplement 1

293 Figure1-figure supplement 2

294 Figure1-figure supplement 3

295 Figure1-figure supplement 4

296 Figure 2

297 Figure2- figure supplement 1

298 Figure 3

299 Figure 4

300 Figure4-figure supplement 1

301 Table 1

302 Table 2

303

References

Bormuth, V., Howard, J., and Schäffer, E. (2007). LED illumination for video-enhanced DIC imaging of single microtubules. J Microsc *226*, 1–5.

Bormuth, V., Varga, V., Howard, J., and Schäffer, E. (2009). Protein friction limits diffusive and directed movements of kinesin motors on microtubules. Science *325*, 870–873.

Bowne-Anderson, H., Zanic, M., Kauer, M., and Howard, J. (2013). Microtubule dynamic instability: a new model with coupled GTP hydrolysis and multistep catastrophe. Bioessays *35*, 452–461.

Brouhard, G.J., Stear, J.H., Noetzel, T.L., Al-Bassam, J., Kinoshita, K., Harrison, S.C., Howard, J., and Hyman, A.A. (2008). XMAP215 Is a Processive Microtubule Polymerase. Cell *132*, 79–88.

Carvalho, P., Gupta, M.L., Jr, Hoyt, M.A., and Pellman, D. (2004). Cell Cycle Control of Kinesin-Mediated Transport of Bik1 (CLIP-170) Regulates Microtubule Stability and Dynein Activation. Dev. Cell *6*, 815–829.

Caudron, F., Andrieux, A., Job, D., and Boscheron, C. (2008). A new role for kinesin-directed transport of Bik1p (CLIP-170) in Saccharomyces cerevisiae. J. Cell. Sci. *121*, 1506–1513.

Coombes, C.E., Yamamoto, A., Kenzie, M.R., Odde, D.J., and Gardner, M.K. (2013). Evolving tip structures can explain age-dependent microtubule catastrophe. Curr. Biol. *23*, 1342–1348.

Cottingham, F.R., and Hoyt, M.A. (1997). Mitotic spindle positioning in Saccharomyces cerevisiae is accomplished by antagonistically acting microtubule motor proteins. The Journal of Cell Biology *138*, 1041–1053.

Gardner, M.K., Zanic, M., Gell, C., Bormuth, V., and Howard, J. (2011). Depolymerizing kinesins

Kip3 and MCAK shape cellular microtubule architecture by differential control of catastrophe. Cell *147*, 1092–1103.

Gell, C., Bormuth, V., Brouhard, G.J., Cohen, D.N., Diez, S., Friel, C.T., Helenius, J., Hyman, A.A., Salser, S., Drechsel, D.N., Unwin, N., and Mitchison, T.J. (1992). Role of GTP hydrolysis in microtubule dynamics: information from a slowly hydrolyzable analogue, GMPCPP. Molecular Biology of the Cell *3*, 1155–1167.

Gell, C., Friel, C.T., Borgonovo, B., Drechsel, D.N., Hyman, A.A., and Howard, J. (2011). Purification of tubulin from porcine brain. Methods Mol. Biol. *777*, 15–28.

Ghaemmaghami, S., Huh, W., Bower, K., Howson, R. W., Belle, A., Dephoure, N., et al. (2003). Global analysis of protein expression in yeast. *Nature*, *425*(6959), 737–741. doi:10.1038/nature02046

Gupta, M.L., Carvalho, P., Roof, D.M., and Pellman, D. (2006). Plus end-specific depolymerase activity of Kip3, a kinesin-8 protein, explains its role in positioning the yeast mitotic spindle. Nat. Cell Biol. *8*, 913–923.

Huyett, A., Kahana, J., Silver, P., Zeng, X., and Saunders, W.S. (1998). The Kar3p and Kip2p motors function antagonistically at the spindle poles to influence cytoplasmic microtubule numbers. J. Cell. Sci. *111*, 295–301.

Hyman, A.A., Salser, S., Drechsel, D.N., Unwin, N., and Mitchison, T.J. (1992). Role of GTP hydrolysis in microtubule dynamics: information from a slowly hydrolyzable analogue, GMPCPP.

Molecular Biology of the Cell *3*, 1155–1167.

Jannasch, A., Bormuth, V., Storch, M., Howard, J., and Schäffer, E. (2013). Kinesin-8 is a low-force motor protein with a weakly bound slip state. Biophys. J. *104*, 2456–2464.

Margolin, G., Goodson, H.V. and Alber, M.S. (2011). Mean-field study of the role of lateral cracks in microtubule dynamics. Phys. Rev. E - Stat. Nonlinear, Soft Matter Phys. *83*, 041905

Mayr, M.I., Hümmer, S., Bormann, J., Grüner, T., Adio, S., Woehlke, G., and Mayer, T.U. (2007). The human kinesin Kif18A is a motile microtubule depolymerase essential for chromosome congression. Current Biology *17*, 488–498.

Miller, R.K., Heller, K.K., Frisen, L., Wallack, D.L., Loayza, D., Gammie, A.E., and ROSE, M.D. (1998). The kinesin-related proteins, Kip2p and Kip3p, function differently in nuclear migration in yeast. Molecular Biology of the Cell *9*, 2051–2068.

Roberts, A.J., Goodman, B.S., and Reck-Peterson, S.L. (2014). Reconstitution of dynein transport to the microtubule plus end by kinesin. eLife *3*, e02641–e02641.

Schäffer, E., Nørrelykke, S.F., and Howard, J. (2007). Surface Forces and Drag Coefficients of Microspheres near a Plane Surface Measured with Optical Tweezers. Langmuir *23*, 3654–3665.

Stumpff, J., Dassow, von, G., Wagenbach, M., Asbury, C., and Wordeman, L. (2008). The kinesin-8 motor Kif18A suppresses kinetochore movements to control mitotic chromosome alignment. Dev. Cell *14*, 252–262.

Tolić-Nørrelykke, S.F., Schäffer, E., Howard, J., Pavone, F.S., Jülicher, F., and Flyvbjerg, H. (2006). Calibration of optical tweezers with positional detection in the back focal plane. Review of Scientific Instruments *77*, 103101.

373 Varga, V., Helenius, J., Tanaka, K., Hyman, A.A., Tanaka, T.U., and Howard, J. (2006). Yeast
374 kinesin-8 depolymerizes microtubules in a length-dependent manner. Nat. Cell Biol. *8*, 957–962.

375 Varga, V., Leduc, C., Bormuth, V., Diez, S., and Howard, J. (2009). Kinesin-8 motors act
376 cooperatively to mediate length-dependent microtubule depolymerization. Cell *138*, 1174–1183.

377 Verde, F., Dogterom, M., Stelzer, E., Karsenti, E., and Leibler, S. (1992). Control of microtubule
378 dynamics and length by cyclin A- and cyclin B-dependent kinases in Xenopus egg extracts. The
379 Journal of Cell Biology *118*, 1097–1108.

380 Widlund, P.O., Podolski, M., Reber, S., Alper, J., Storch, M., Hyman, A.A., Howard, J., and
381 Drechsel, D.N. (2012). One-step purification of assembly-competent tubulin from diverse
382 eukaryotic sources. Molecular Biology of the Cell *23*, 4393–4401.
383
384 Widlund, P.O., Stear, J.H., Pozniakovsky, A., Zanic, M., Reber, S., Brouhard, G.J., Hyman,
385 A.A., and Howard, J. (2011). XMAP215 polymerase activity is built by combining multiple
386 tubulin-binding TOG domains and a basic lattice-binding region. Proc. Natl. Acad. Sci. U.S.a.
387 *108*, 2741–2746.
388
389 Wieczorek, M., Bechstedt, S., Chaaban, S., and Brouhard, G.J. (2015). Microtubule-associated
390 proteins control the kinetics of microtubule nucleation. Nat. Cell Biol. *17*, 907–916.

391

392 **Acknowledgements**

393 We thank T. Hyman, S. Diez and S. Alberti for guidance; M. Podolski for the kind gift of yeast
394 tubulin; J. Alper for critical reading of earlier versions of the manuscript; H. Petzold for technical
395 help with protein expression and assays; and members of the Howard and Diez laboratories for

396 discussions, reading, and feedback. We would like to thank the following Services and Facilities
397 of the MPI-CBG for their support: Protein Expression, Chromatography and Mass spectrometry.
398 There are no potential conflicts of interest. AH & AJ performed experiments with technical
399 support from AB & MM, MS & DL made preliminary observations, the data were analyzed by
400 AH, AJ, ES & JH and AH & JH wrote the paper. Research reported in this publication was
401 supported by the Max Planck Society, an ERC Starting Grant 2010 (Nanomech 260875) to AJ &
402 ES, and by the NIGMS of the National Institutes of Health under award number R01GM110386
403 to JH. The content is solely the responsibility of the authors and does not necessarily represent
404 the official views of the National Institutes of Health.
405
406

Figure Legends

Figure 1. Kip2 is a microtubule polymerase and an anti-catastrophe factor on porcine tubulin.

A Schematic of the experimental design: porcine tubulin (green) polymerizes onto stabilized microtubules (red) bound to the coverslip with antibodies (blue), imaged using TIRF microscopy. **B** Microscopy images of dynamic microtubules grown from stabilized seeds without (left) and with 40 nM Kip2 (right) at t = 10 minutes. **C** Microtubule length as a function of Kip2 concentration in ATP (black circles) or AMP-PNP (blue circles) at t = 10 ten minutes. The red line indicates the expected microtubule length at t = 10 minutes, calculated from the measured growth rates and catastrophe frequencies in Table 1 according to the formula $L = (v_+/f_{+-})[1-\exp(-tf_{+-})]$, where v_+ is the growth rate and f_{+-} is the catastrophe frequency (ignoring rescues and assuming that regrowth occurs without delay). **D** Kymographs showing typical microtubule growth without (left) and with 5 nM Kip2 (right) in ATP. **E** Microtubule growth rate as a function of Kip2 concentration in ATP. **F** Catastrophe frequency as a function of Kip2 concentration in ATP. All error bars are standard errors of the mean. Please refer to Table 1 for values.

Figure1-figure supplement 1. Kip2 has no significant effect on microtubule shrinkage rate but increases rescue distance

A Porcine microtubule length at 0 or 40 nM Kip2-eGFP in ATP, measured at t = 10 minutes. **B** Porcine microtubule shrinkage rate as a function of Kip2 concentration. The grey box indicates the Kip2 concentration regime in which microtubule catastrophe is very rare and we did not quantify microtubule shrinkage rate. The data were fitted by linear regression, weighted by the SE. Slope = 0.09 ± 0.11, y-intercept = 28.1 ± 0.58 μm/min. **C** Porcine microtubule rescue frequency (shrinkage rate divided by rescue distance) as a function of Kip2 concentration. The grey box indicates the Kip2 concentration regime in which microtubule catastrophe is very rare

and we did not measure shrinkage rate or rescue frequency. The data were fitted by linear regression, weighted by the SE. Slope = 0.0081 ± 0.0014, *y*-intercept = 0.01 ± 0.01 μm. Error bars are SE.

Figure1-figure supplement 2. Kip2 is a microtubule polymerase and an anti-catastrophe factor on yeast tubulin

A Kymographs from DIC microscopy showing typical microtubule growth with 4 μM unlabeled yeast tubulin without (left) and with Kip2 (5 nM, center, 20 nM, right) in ATP. **B** Yeast microtubule growth rate as a function of Kip2 concentration in ATP. **C** Catastrophe frequency as a function of Kip2 concentration of yeast microtubules in ATP. Error bars are SE. Please refer to Table 2 for values.

Figure1-figure supplement 3. Kip2 increases the growth rate in GTP-tubulin and lowers the off-rate of GMPCPP-tubulin.

A Porcine microtubule growth rate from GMPCPP seeds as a function of tubulin concentration in ATP without Kip2 (red) and with 40 nM Kip2 (black) in solution. The data were fit using linear regression, weighted by the SE. The slope corresponds to a second-order association rate for free GTP-tubulin dimers of 0.70 ± 0.30 $\mu M^{-1} \cdot s^{-1}$ without Kip2 and 1.48 ± 0.16 $\mu M^{-1} \cdot s^{-1}$ with 40 nM Kip2. The *y*-intercepts were -1.9 ± 4.0 s^{-1} without Kip2 and -0.21 ± 1.6 s^{-1} with 40 nM Kip2; the intercepts did not differ significantly from zero. **B** Shrinkage rates of GMPCPP microtubules at 0 nM Kip2 (light grey) and 40 nM Kip2 (dark grey) in ATP and AMP-PNP. Error bars are SEs.

Figure1-figure supplement 4. SDS-PAGE gels of Kip2 and Kip2-eGFP.

Lane 1: Pooled Kip2 fractions after gel filtration (78 kDa). Lane 2: Pooled Kip2-eGFP fractions after gel filtration (105 kDa). Molecular weight markers (Seeblue® Plus2) are indicated by horizontal lines.

Figure 2. Kip2 is a highly processive, weak motor that dwells at plus-ends.

A Schematic of the experimental design. **B** Kymograph showing processive motility and plus-end accumulation of individual Kip2-eGFP molecules on GMP-CPP stabilized microtubules in 1 mM ATP. The concentration of Kip2-eGFP was 0.085 nM. **C** Kymograph showing tightly bound Kip2-eGFP molecules in AMP-PNP. **D** Kymograph showing end-residence of individual Kip2-eGFP molecules in ATP.**E** Kymograph showing end-residence of 1 nM Kip2-eGFP spiked into 20 nM unlabeled Kip2 in the presence of 8 µM unlabeled tubulin in ATP. Arrow heads indicate microtubule plus-end tracking events.

Figure2-figure supplement 1. Kip2-eGFP velocity, run-length and end-residence time distributions.

A Histogram showing velocities of single Kip2-eGFP molecules on GMPCPP-stabilized porcine microtubules in 1 mM ATP. **B** Histogram showing the distribution of Kip2-eGFP run-lengths on GMPCPP-stabilized porcine microtubules in 1 mM ATP. The run-length of Kip2 is predicted to be exponentially distributed, as dissociation from the microtubule lattice is expected to be a random process. The red line depicts a single exponential: $f(x) = A \exp(-x/x_0)$, where A = 21.1 ± 2.1 and x_0 = 3.6 ± 1.0 µm; run-lengths between 0 and 0.5 µm are under-represented, likely due to the limited temporal resolution. **C** Histogram showing end-residence times of Kip2-eGFP on GMPCPP-stabilized porcine microtubules. End-residence times were included in the analysis only if single Kip2-eGFP molecules could be observed to arrive at, and dissociate from, a

481 microtubule plus-end. The red line depicts a single exponential: $f(t) = A \exp(-t/t_0)$, where A =
482 18.2 ± 2.4 and t_0 = 44.1 ± 14.5 s.
483
484 **Figure 3. Kip2 is a low-force motor**
485 A Stall force measurement tace. Sampling rate: 10 kHz, raw data (gray), box car filtered to 50
486 Hz (black). A force of 0.5 N corresponds to a displacement of about 17 nm. B Time trace for a
487 slip event under 3 pN hindering (load) force. Sampling rate: 20 kHz, raw data (light cyan),
488 boxcar filtered to 400 Hz (dark cyan). C Kip2 force-velocity curve: positive is a hindering (load)
489 force and negative is an assisting force. Open symbols include slip events. Error bars are SE.
490
491 **Figure 4. Kip2 promotes porcine microtubule growth in a length-dependent manner.**
492 **A** Kymograph showing acceleration of microtubule growth with increasing length at 40 nM Kip2.
493 **B** Porcine microtubule growth rate as a function of length without Kip2 (black) and binned for 1-
494 2 nM Kip2 (purple), 5-10 nM Kip2 (blue) and 20-40 nM Kip2 (green). Lengths are binned for 0-2
495 µm, 2-3 µm, 3-4 µm, 4-6 µm, 6-8 µm, 8-12 µm, 12-16 µm and 16-24 µm. The data were fit with
496 the equation: $v(L) = v_0 + (v_{max} - v_0)\,[\text{Kip2}]L / ([\text{Kip2}]L + A)$, where v_0 = 0.294 ± 0.009 µm/min is
497 the initial growth rate, v_{max} = 1.03 ± 0.03 µm/min is the maximum growth rate, L is microtubule
498 length and A = 39.8 ± 5.4 µm·nM. The parameter values for yeast microtubules are: v_0 = 0.238
499 ± 0.005 µm/min, v_{max} = 0.78 ± 0.02 µm/min and A = 79.4 ± 8.7 µm·nM. **C** Mean catastrophe
500 length at various Kip2 concentrations for short (light grey) and long (dark grey) microtubules. In
501 the short microtubule bins, we summed the total distance that microtubules grew while shorter
502 than 4 µm and divided by the number of catastrophes that occurred at lengths < 4 µm. In the
503 long microtubule bin, we summed the total distance that microtubules grew while longer 4 µm
504 and divided by the number of catastrophes that occurred at lengths > 4 µm (Figure 4C, inset).
505 The number of catastrophes was 120 (0 nM Kip2), 102 (1 nM Kip2), 111 (2 nM Kip2) and 23 (5

nM Kip2). The number of catastrophes at higher Kip2 concentrations was too small to make statistically significant comparisons. Error bars are SEs.

Figure4-figure supplement 1. Length dependence of growth and catastrophe for yeast tubulin

A Yeast microtubule growth rate as a function of length, without Kip2 (black) and binned for 5-10 nM Kip2 (blue) and 20-40 nM Kip2 (green). Lengths are binned for 0-2 μm, 2-3 μm, 3-4 μm, 4-6 μm, 6-8 μm, 8-12 μm, 12-16 μm and 16-24 μm. The data were fit with the equation: $v(L) = v_0 + (v_{max} - v_0)\,[Kip2]L / ([Kip2]L+A)$, where v_0 = 0.238 ± 0.005 μm/min is the initial growth rate, v_{max} = 0.78 ± 0.02 μm/min is the maximum growth rate, L is microtubule length and A = 79.4 ± 8.7 μm·nM. **B** Mean length at catastrophe for yeast microtubules at 0 nM Kip2 (n = 170 catastrophes), 5 nM Kip2 (n = 101) and 10 nM Kip2 (n = 80). Bars depict dynamic microtubule lengths below 4 μm (light grey) or above 4 μm (dark grey). Error bars are SE.

Table 1. Parameters of microtubule dynamics for 12 μM porcine tubulin (mean ± SE)

[Kip2] (nM)	Length (μm)	Growth rate (μm/min)	Catastrophe frequency (min^{-1})	Catastrophe distance[a] (μm)	Shrinkage rate (μm/min)	Rescue frequency (min^{-1})	Rescue distance[b] (μm)
0	0.99 ± 0.12 (*n* = 54)	0.32 ± 0.02 (*n* = 172)	0.166 ± 0.015 (*n* = 126)	1.93 ± 0.21	27.6 ± 0.96 (*n* = 130)	0.88 ± 0.38 (*n* = 7)	31.5 ± 11.9 (*n* = 7)
1	1.0 ± 0.16 (*n* = 75)	0.37 ± 0.01 (*n* = 152)	0.126 ± 0.012 (*n* = 104)	2.94 ± 0.30	27.7 ± 0.85 (*n* = 85)	0.20 ± 0.71 (*n* = 2)	140.7 ± 99.5 (*n* = 2)
2	2.1 ± 0.16 (*n* = 88)	0.35 ± 0.01 (*n* = 159)	0.135 ± 0.013 (*n* = 115)	2.59 ± 0.25	29.7 ± 0.89 (*n* = 110)	0.54 ± 0.45 (*n* = 5)	55.4 ± 24.8 (*n* = 5)
5	5.3 ± 0.21 (*n* = 82)	0.62 ± 0.03 (*n* = 77)	0.065 ± 0.011 (*n* = 33)	9.5 ± 1.7	28.4 + 1.76 (*n*= 45)	2.2 ± 0.41 (*n* = 9)	13.1 ± 4.4 (*n* = 9)
10	6.4 ± 0.19 (*n* = 75)	0.78 ± 0.03 (*n* = 38)	0.043 ± 0.011 (*n* = 16)	18.1± 4.6	28.9 ± 4.1 (*n* = 18)	1.8 ± 0.41 (*n* = 6)	15.9 ± 6.5 (*n* = 6)
20	7.7 ± 0.28 (*n* = 68)	0.99 ± 0.04 (*n* = 36)	0.020 ± 0.006 (*n* = 10)	49.5 ± 0.10	-	-.	-
40	8.8 ± 0.64 (*n* = 26)	0.94 ± 0.05 (*n* = 18)	0.004 ± 0.004 (*n* = 1)	235.0 ± 1.0	-	-	-

[a]The catastrophe distance is the growth rate divided by the catastrophe frequency.

[b]The rescue distance is the shrinkage rate divided by the rescue frequency.

529 **Table 2. Parameters of microtubule dynamics for 4 µM yeast tubulin (mean ± SE)**

[Kip2] (nM)	**Growth rate (µm/min)**	**Catastrophe frequency (min^{-1})**
0	0.257 ± 0.004 (*n* = 300)	0.234 ± 0.017 (*n* = 191)
5	0.302 ± 0.005 (*n* = 263)	0.137 ± 0.012 (*n* = 141)
10	0.353 ± 0.008 (*n* = 146)	0.103 ± 0.010 (*n* = 116)
20	0.572 ± 0.01 (*n* = 57)	0.020 ± 0.006 (*n* = 13)
40	0.589 ± 0.012 (*n* = 48)	0.009 ± 0.004 (*n* = 5)

530

531

532

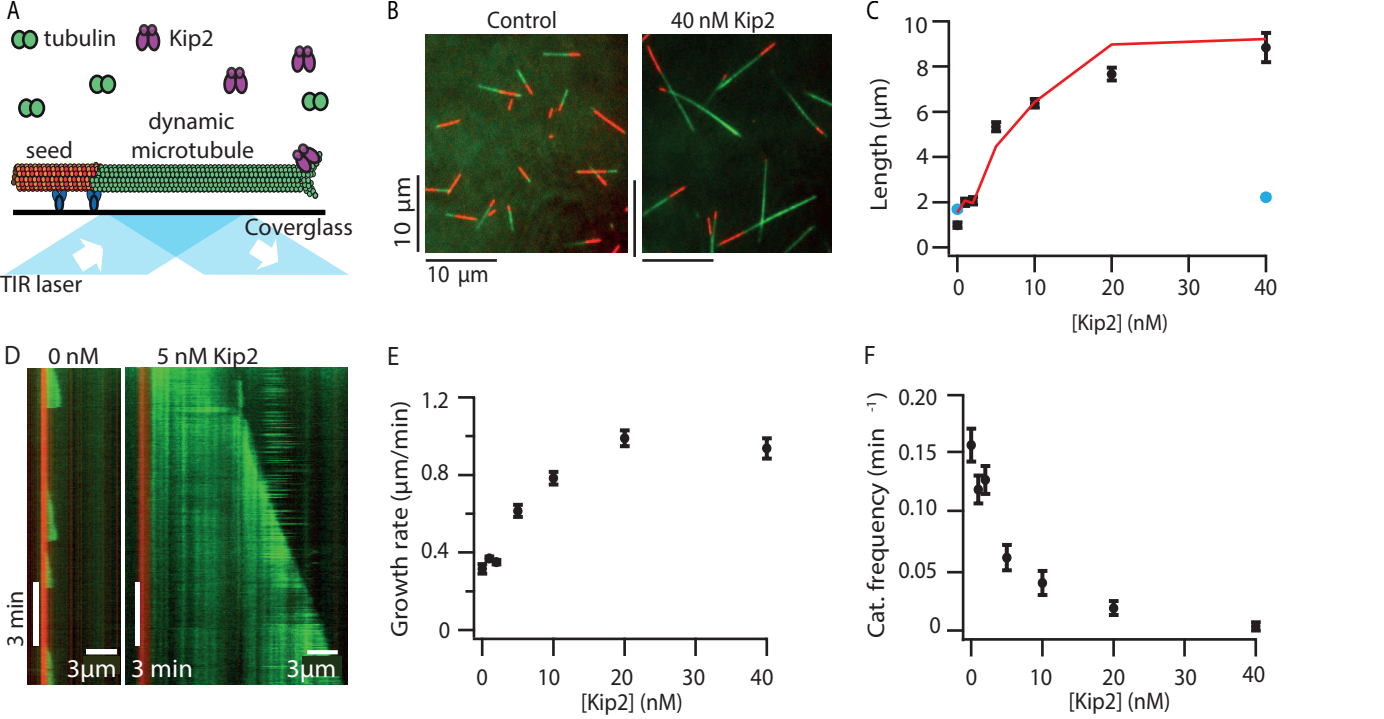
A
tubulin
Kip2
dynamic
microtubule
seed
Coverglass
TIR laser
B
Control
40 nM Kip2
10 µm
10 µm
C
Length (µm)
[Kip2] (nM)
D
0 nM
5 nM Kip2
3 min
3µm
3 min
3µm
E
Growth rate (µm/min)
[Kip2] (nM)
F
Cat. frequency (min -1)
[Kip2] (nM)

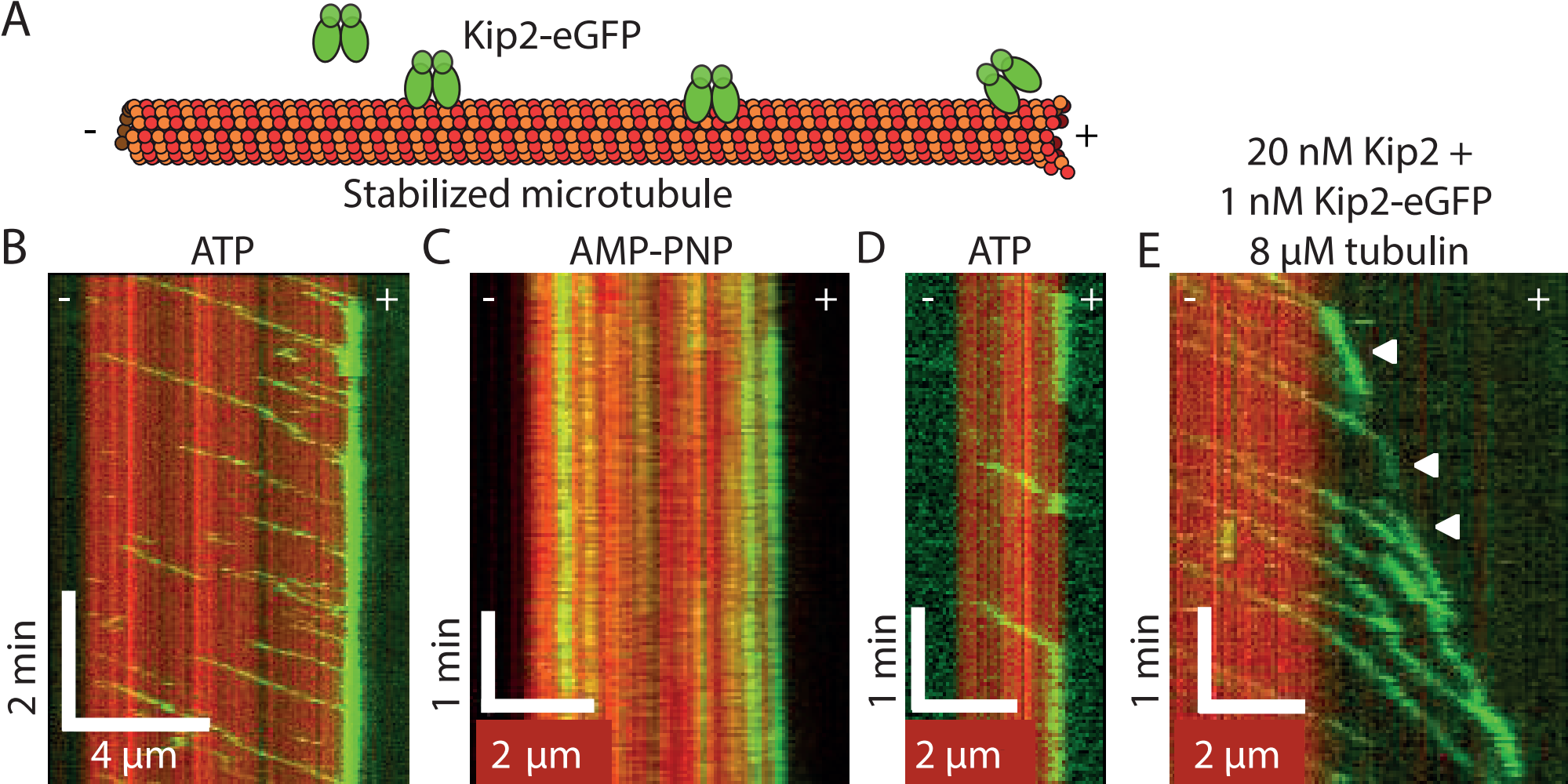
A
Kip2-eGFP
-
+
Stabilized microtubule
B
ATP
C
AMP-PNP
D
ATP
E
20 nM Kip2 +
1 nM Kip2-eGFP
8 µM tubulin
2 min
4 µm
1 min
2 µm
1 min
2 µm
1 min
2 µm

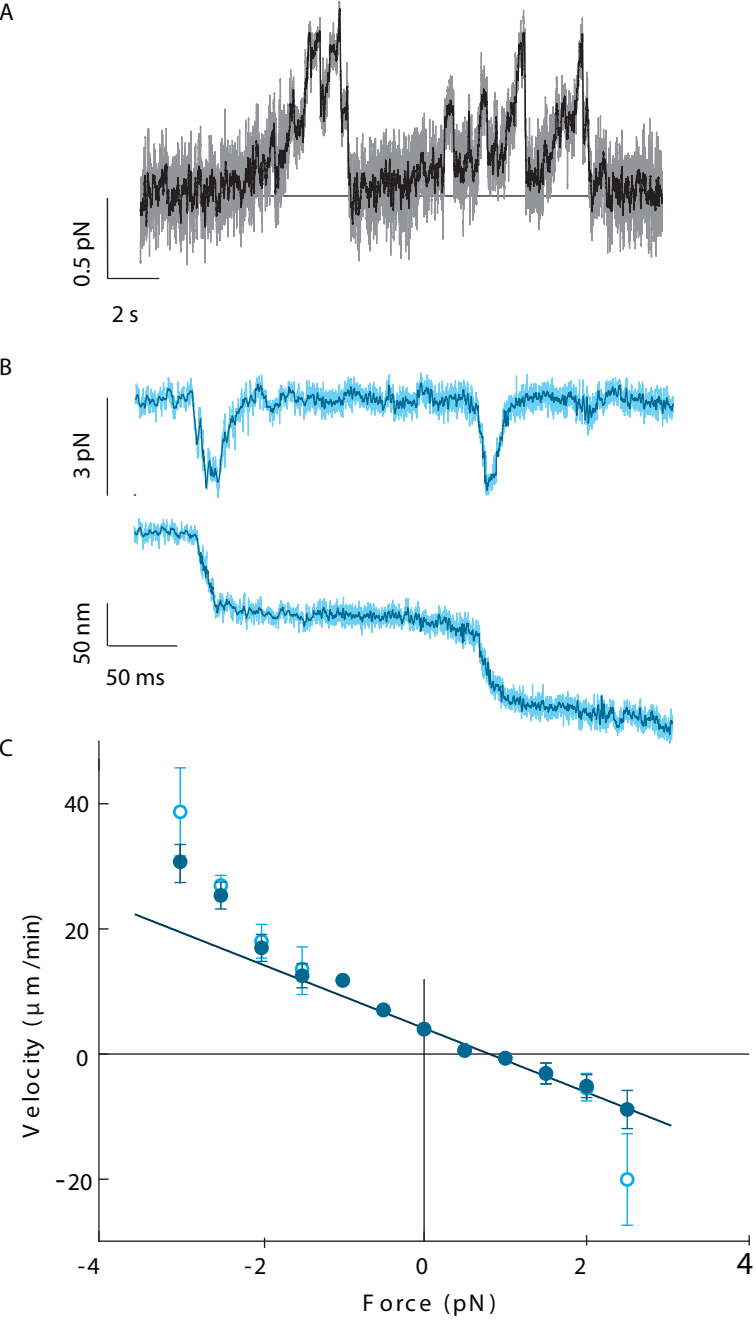
A
0.5 pN
2 s
B
3 pN
50 nm
50 ms
C
40
20
0
-20
Velocity (μm/min)
-4
-2
0
2
4
Force (pN)

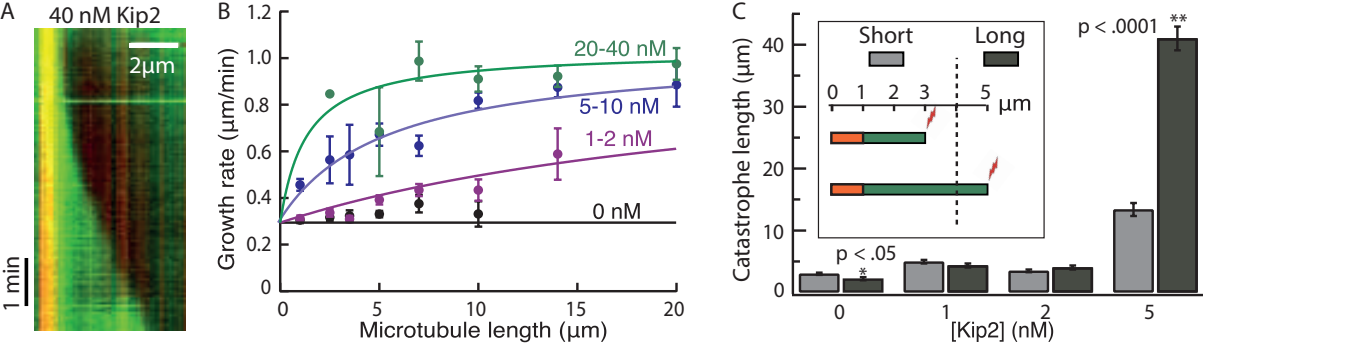
A
40 nM Kip2
2μm
1 min
B
Growth rate (μm/min)
Microtubule length (μm)
20-40 nM
5-10 nM
1-2 nM
0 nM
C
Catastrophe length (μm)
[Kip2] (nM)
Short
Long
μm
p < .0001
**
p < .05
*

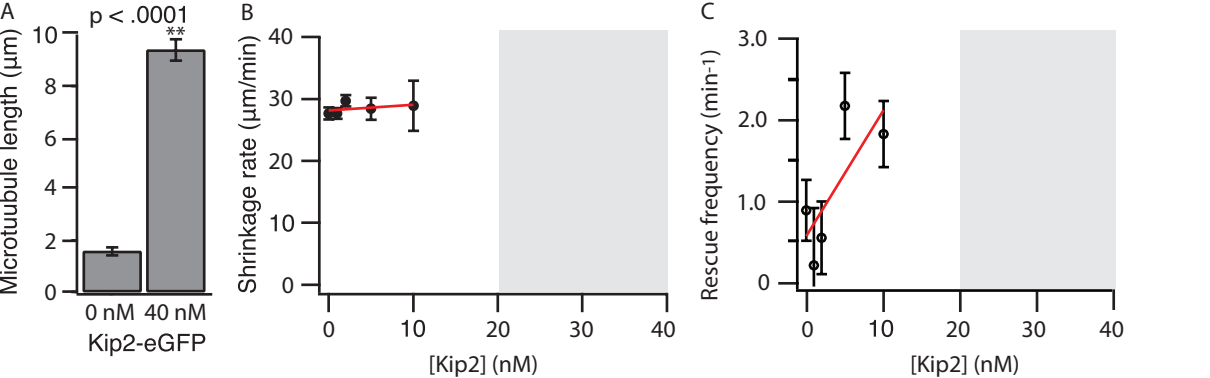
A
p < .0001
**
Microtuubule length (µm)
10
8
6
4
2
0
0 nM
40 nM
Kip2-eGFP
B
Shrinkage rate (µm/min)
40
30
20
10
0
0
10
20
30
40
[Kip2] (nM)
C
Rescue frequency (min-1)
3.0
2.0
1.0
0
0
10
20
30
40
[Kip2] (nM)

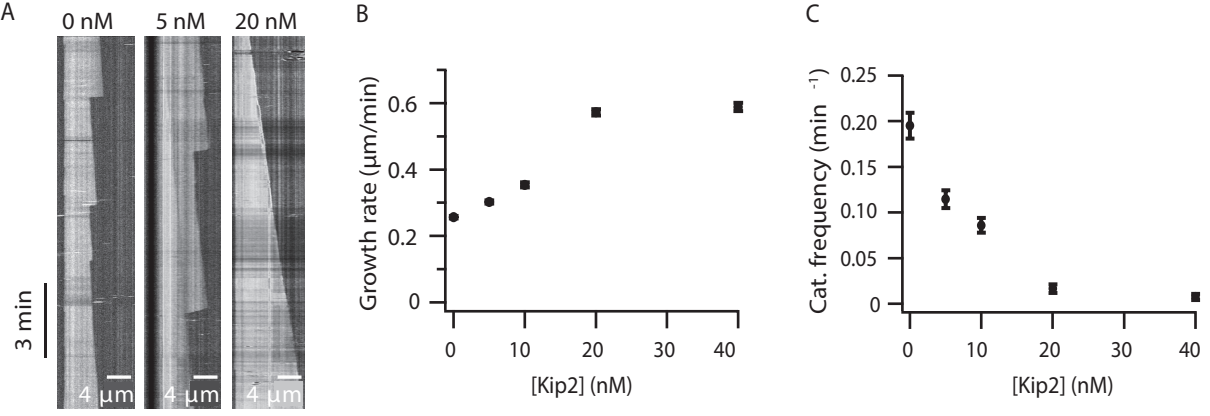
A
0 nM
5 nM
20 nM
3 min
4 µm
4 µm
4 µm
B
Growth rate (µm/min)
0
0.2
0.4
0.6
0
10
20
30
40
[Kip2] (nM)
C
Cat. frequency (min -1)
0
0.05
0.10
0.15
0.20
0.25
0
10
20
30
40
[Kip2] (nM)

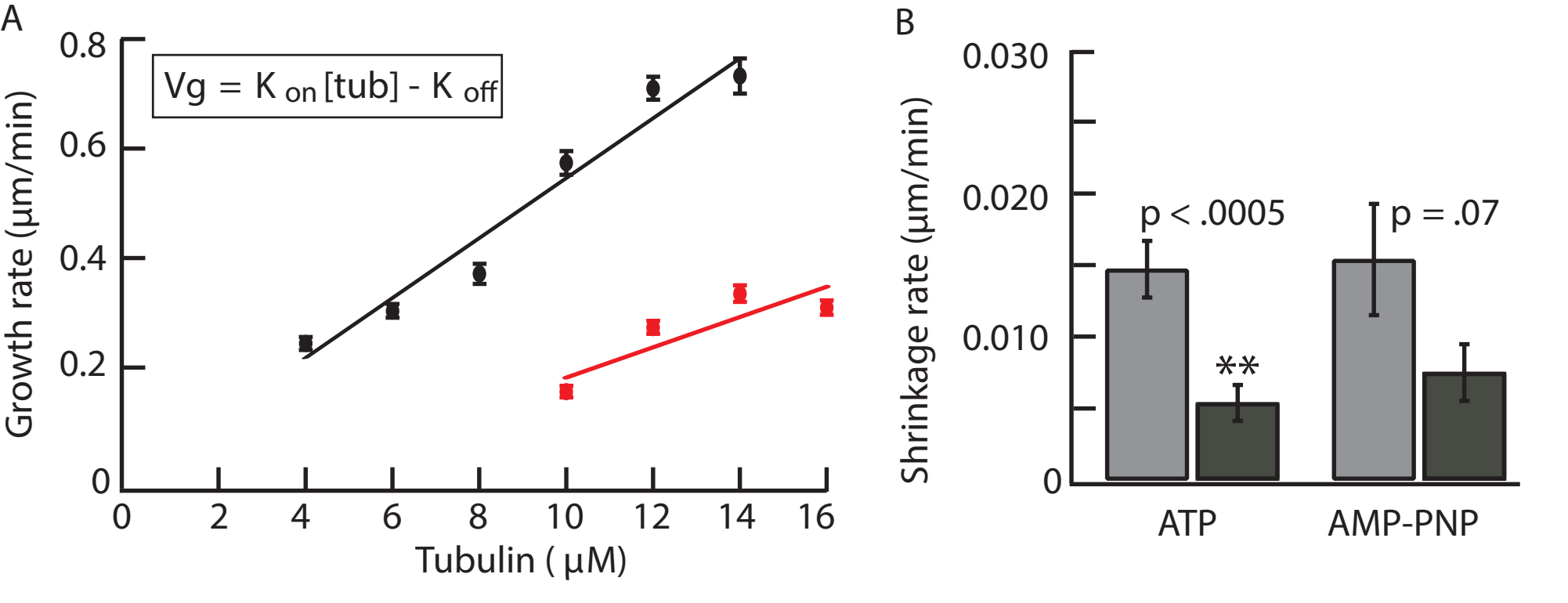
A
Vg = K on [tub] - K off
Growth rate (µm/min)
0.8
0.6
0.4
0.2
0
0
2
4
6
8
10
12
14
16
Tubulin (µM)
B
Shrinkage rate (µm/min)
0.030
0.020
0.010
0
p < .0005
**
p = .07
ATP
AMP-PNP

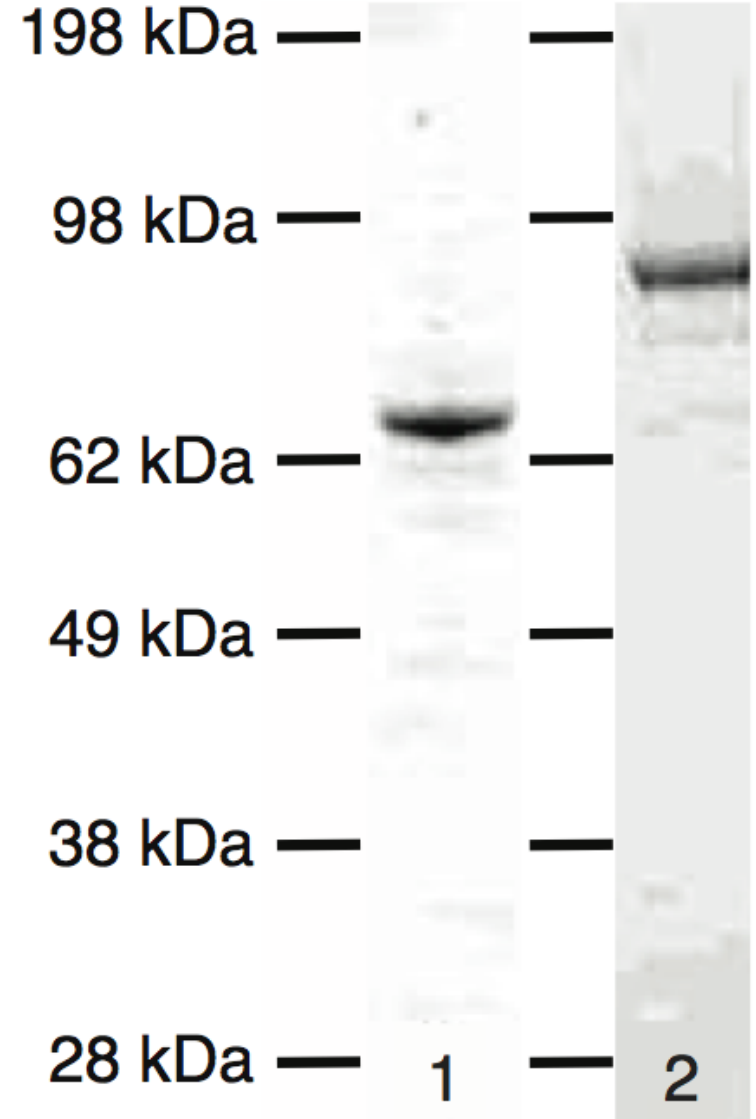
198 kDa
98 kDa
62 kDa
49 kDa
38 kDa
28 kDa
1
2

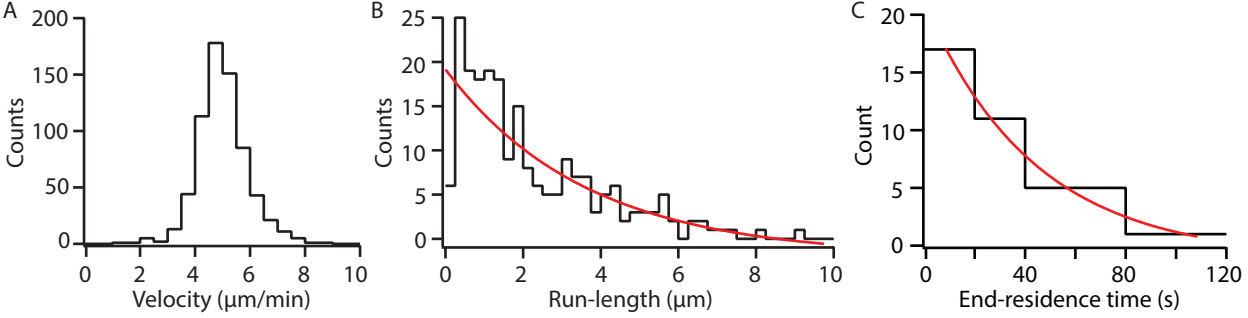
A
Counts
200
150
100
50
0
0
2
4
6
8
10
Velocity (μm/min)
B
Counts
25
20
15
10
5
0
0
2
4
6
8
10
Run-length (μm)
C
Count
20
15
10
5
0
0
40
80
120
End-residence time (s)

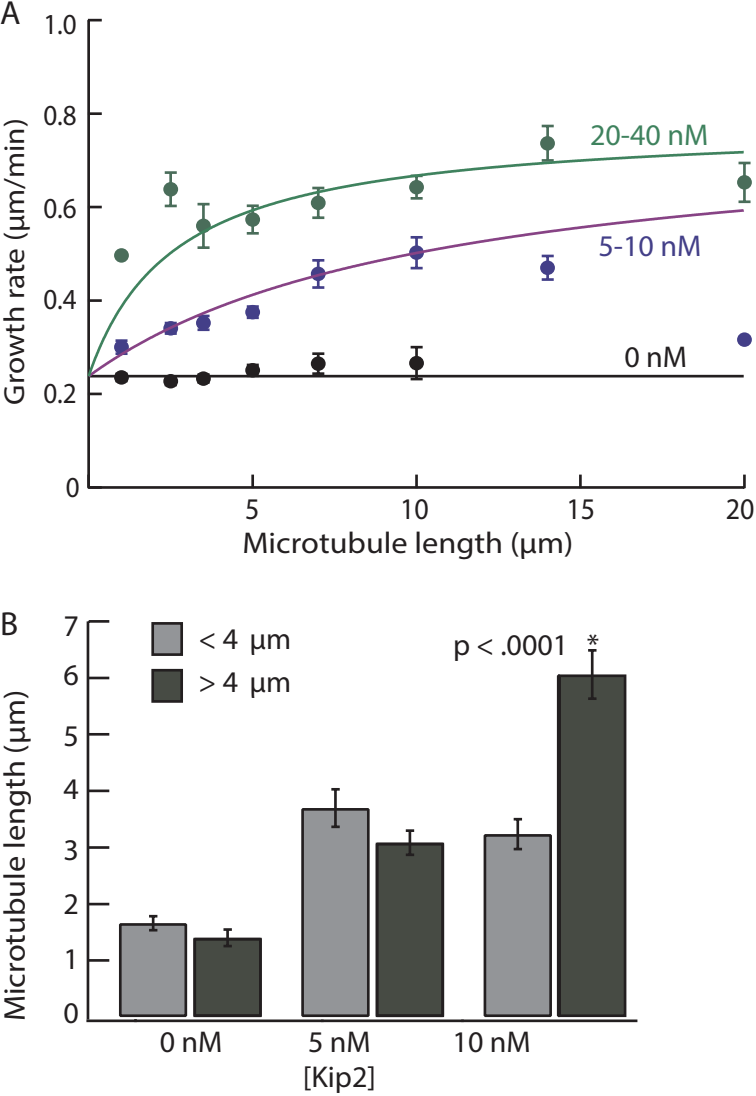
A
1.0
0.8
0.6
0.4
0.2
0
Growth rate (μm/min)
20-40 nM
5-10 nM
0 nM
5
10
15
20
Microtubule length (μm)
B
7
6
5
4
3
2
1
0
Microtubule length (μm)
< 4 μm
> 4 μm
p < .0001 *
0 nM
5 nM
10 nM
[Kip2]